ACS APPLIED MATERIALS & INTERFACES

www.acsami.org

Research Article

Chemiluminescent Two-Dimensional Metal–Organic Framework with Multiple Metal Catalytic Centers and Its Peroxidase-like Activity for Sensing of Small Molecules

Jue Wang, Chao Hu, Yi-sha Wang, and Hua Cui*

Cite This: *ACS Appl. Mater. Interfaces* 2022, 14, 3156–3164

Read Online

ACCESS | Metrics & More | Article Recommendations | Supporting Information

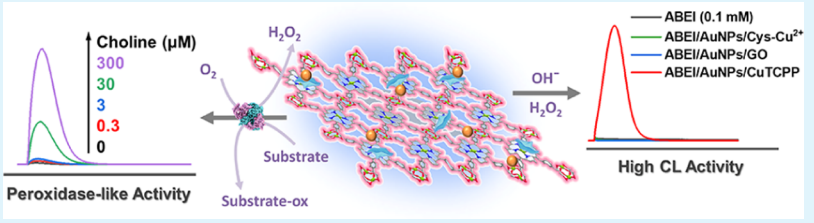

ABSTRACT: Two-dimensional (2D) porphyrin-based metal–organic frameworks (MOFs) hold great promise in a variety of areas with the merits of large lateral size and abundant functional groups. The chemiluminescent 2D MOF has rarely been reported. In this work, a chemiluminescence (CL) reagent and noble metal nanoparticle dual-functionalized 2D MOF (ABEI/AuNPs/CuTCPP) was developed through the surfactant-assisted and *in situ* synthetic growth method, exhibiting strong and stable CL property and outstanding peroxidase-mimicking activity. The special nanostructure of ABEI/AuNPs/CuTCPP endowed it with multi-catalytic routes in the CL reaction, which showed a unique pH-regulated and time-resolved CL kinetic curve. A CL mechanism with multi-catalytic centers has been proposed. AuNPs participated in the fast catalytic process and CuTCPP in the slow and strong catalytic reaction. Owing to the impressive structural features and intrinsic enzymatic tandem reaction from natural enzyme to artificial enzyme, a model biosensor was designed for the detection of small metabolic molecules. Employing choline as a model target, the proposed biosensor showed a highly sensitive response to choline in the linear range from 0.3 to 300 μM with a detection limit of 82.6 nM. Significantly, the strategy may be generalized to the monitoring of other biologically important compounds involved in the production of H_2O_2.

KEYWORDS: *2D metal–organic frameworks, chemiluminescence, functionalized nanomaterials, porphyrin chemistry, sensing, small molecules*

INTRODUCTION

Nanomaterial-assisted chemiluminescence (CL) systems have been strongly advanced for years to enhance CL intensity and to achieve ultrasensitive analytical performance.[1−3] Metal–organic frameworks (MOFs), as a tempting class of crystalline nanoporous materials, are predicted to be highly attractive for the applications in CL due to their large specific surface area, extensive porosity, tunable structures, flexible functionalities, and catalytic active centers.[4−6] Till date, most reports generally focus on either MOF-catalyzed liquid-phase CL systems,[7,8] which is not convenient for acting as biolabeling directly, or MOF-participated peroxyoxalate CL systems,[9,10] which occur in organic environments and limit their applications. Even though several chemiluminescent-functionalized MOFs have been developed,[11,12] the preparation procedure is often complicated, and their study on CL behavior is still in its infancy. Therefore, it is highly desired to fabricate chemiluminescent MOF nanocomposites with superior CL activity and remarkable sensing abilities.

The porphyrin-based MOF is an important branch which is endowed with rigid geometry and prominent properties. Porphyrin molecules are macrocyclic molecules with stable π-conjugated architectures and terminal functional groups. On the other hand, their tendency of metalation[13] is favorable for imbuing the parent MOF with unsaturated metal centers which are crucial to the enhancement of CL property. Especially, an ultrathin two-dimensional (2D) porphyrin-based MOF was reported to show better performance than conventional three-dimensional (3D) MOFs, in terms of dispersity, exposure degree of active sites, and mass transfer.[14,15] Considering that high-density exposure of active metal sites and π-conjugated

Received: October 18, 2021
Accepted: December 26, 2021
Published: January 4, 2022

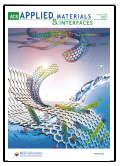

https://doi.org/10.1021/acsami.1c20092
ACS Appl. Mater. Interfaces 2022, 14, 3156–3164

Scheme 1. Schematic Illustration for Synthesis of ABEI/AuNPs/CuTCPP

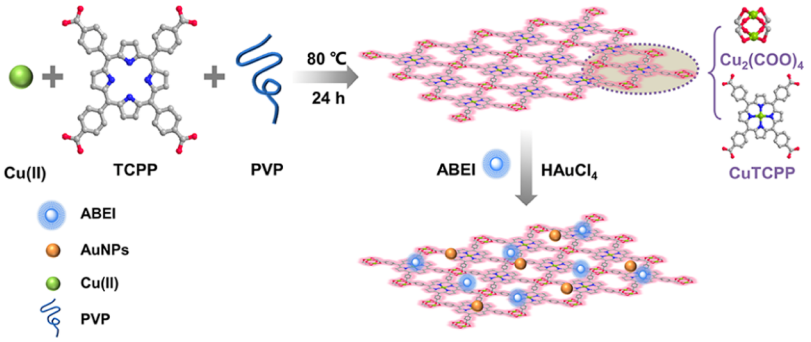

platform with large specific surface area and abundant functional groups in 2D porphyrin-based MOF, an appealing route for versatile 2D MOF-based nanocomposites is to integrate them with other active components like nanoparticles, quantum dots, enzymes, and so forth,[16−18] showing comprehensive performance. However, 2D porphyrin-based MOF nanocomposites with multi-catalytic centers for the CL reactions have rarely been disclosed. By coupling 2D MOF with CL reagents and multi-catalysts, there stands a good chance for us to design novel CL-functionalized nanocomposites with multi-catalytic centers.

As essential participants in living organisms, small biomolecules, such as choline, glucose, and lactic acid, play vital roles in the prevention or progression of various health issues. Changes in the choline level will reflect the state of metabolism, apoptosis, material transfer, and signal transmission, thus can be used as a diagnosis indicator of multiple diseases. For example, the abnormal concentration of choline usually indicates the risk of neurological diseases like Alzheimer's and Parkinson's disease.[19,20] These small biomolecules will react with ambient O_2 assisted by the corresponding oxidase (choline oxidase, glucose oxidase, lactate oxidase, *etc.*). Biosensors based on the bienzymatic system [*e.g.,* choline oxidase (ChO*x*) and peroxidase (HRP)] are highly selective and sensitive but costly and easy to denaturation. Therefore, it is in high demand to develop simple, cost-effective, and rapid-response biosensors for the monitoring of small biomolecules in bodily fluids.

Herein, we present a CL-functionalized 2D porphyrin-based MOF nanocomposites through the surfactant-assisted and *in situ* growth synthetic method. During the synthesis process, CuTCPP nanosheets served as a nanoplatform with plenty of functional groups and large specific areas, *N*-(4-aminobutyl)-*N*-ethylisoluminol (ABEI) functioned as reductive reagents and CL species, Au(III) was *in situ* reduced to AuNPs, and ABEI was assembled on the surfaces of AuNPs and CuTCPP, forming ABEI/AuNPs/CuTCPP nanocomposites. The nanocomposites exhibited strong and stable CL property with pH-regulated and time-resolved CL kinetic curves. The effect of pH and radical scavengers on the CL behavior was studied. A CL mechanism with multi-catalytic centers has been proposed. Based on the intrinsic peroxidase-mimicking activity of ABEI/AuNPs/CuTCPP nanocomposites, a model biosensor was developed for the detection of small biomolecules involved in the production of H_2O_2 during metabolic processes.

EXPERIMENTAL SECTION

Chemicals. Tetrakis(4-carboxyphenyl)porphyrin (TCPP) and *N*-(4-aminobutyl)-*N*-ethylisoluminol (ABEI) were purchased from Tokyo Chemical Industry Co., Ltd. (Tokyo, Japan). ABEI stock solution was prepared by dissolving ABEI in 0.1 M NaOH solution and kept at 4 °C for further experiments. Polyvinyl pyrrolidone (PVP-K30) and copper nitrate trihydrate ($Cu(NO_3)_2{\cdot}3H_2O$) were purchased from J&K Scientific Ltd. (Beijing, China). Trifluoroacetic acid and pyrazine were purchased from Aladdin Industrial Corporation (Shanghai, China). Choline oxidase (ChO*x*, 50 units) was purchased from Sigma-Aldrich (St. Louis, USA) and dissolved in K_2HPO_4−KH_2PO_4 buffer (0.1 M, pH = 8.0) for 5 mg/mL stock solution. 30% (v/v) H_2O_2 was purchased from Xinke Electrochemical Reagent Factory (Bengbu, China), and H_2O_2 reaction solution was prepared freshly in alkaline solution before CL measurements. Other unmentioned reagents were all purchased from Sinopharm Chemical Reagent Co., Ltd. (Shanghai, China). Ultrapure water was prepared by a Milli-Q system (Millipore, France) and used throughout the experiments. All the reagents used in the study were of analytical grade.

Synthesis of Dual-Functionalized CL Nanocomposites (ABEI/AuNPs/MOFs). 2D porphyrin-based MOFs (M-TCPP) and classic 3D MOFs [HKUST-1, MIL-53(Fe)] were prepared according to the literatures.[21−23] Detailed descriptions are listed in Supporting Information, Section S1. ABEI/AuNPs/CuTCPP were prepared as follows: 10 mM $HAuCl_4$ was added into the obtained CuTCPP mixtures at a volume ratio of 1:100. After continuous stirring for 2 h, 10 mM ABEI solution was added and proceeded for 12 h. The resulting mixtures were centrifuged at 10,000 rpm for 10 min and washed with EtOH to remove unreacted precursor components. Finally, purified ABEI/AuNPs/CuTCPP nanocomposites were obtained. For control experiments, other functionalized 2D MOFs (ABEI/AuNPs/M-TCPP, where M = Cd, Co, Zn) and 3D MOFs [ABEI/AuNPs/HKUST-1 and ABEI/AuNPs/MIL-53(Fe)] were prepared through the same method without amendment.

Characterizations of ABEI/AuNPs/CuTCPP Nanocomposites. The ABEI/AuNPs/CuTCPP nanocomposites were characterized using a UV−visible spectrophotometer (UV−vis, Agilent 8453, Agilent Technologies, USA), a fluorescence spectrophotometer (FL, F-7000, Hitachi, Japan) equipped with a 150 W Xenon lamp as the light source, Fourier transform infrared spectroscopy (FTIR, EQUINX55, Bruker, Germany), a field emission source transmission electron microscope (JEM-2100F, JEOL, Japan), atomic force microscopy (AFM, Multimode V, Veeco, USA), inductively coupled plasma-atomic emission spectroscopy (ICP-AES, OPTIMA 7000DV, PerkinElmer, USA), X-ray diffraction spectroscopy (XRD, TTR-III, Rigaku, Japan), X-ray photoelectron spectroscopy (XPS, ESCALAB 250, Thermo-VG Scientific, UK) with Al Kα radiation as the X-ray source, and an adsorption analyzer (Micromeritics ASAP2010). The prepared nanocomposites were purified by multiple centrifugations and re-dispersion with EtOH in order to obtain valid surface information of ABEI/AuNPs/CuTCPP by various characterization methods. The precipitates were dried under vacuum at 60 °C for XRD, FTIR, and adsorption experiments or re-dispersed in H_2O for UV−vis and FL analysis. The dispersion was dripped on designated substrates and dried naturally at room temperature for TEM, AFM, and XPS characterizations.

https://doi.org/10.1021/acsami.1c20092
ACS Appl. Mater. Interfaces 2022, 14, 3156−3164

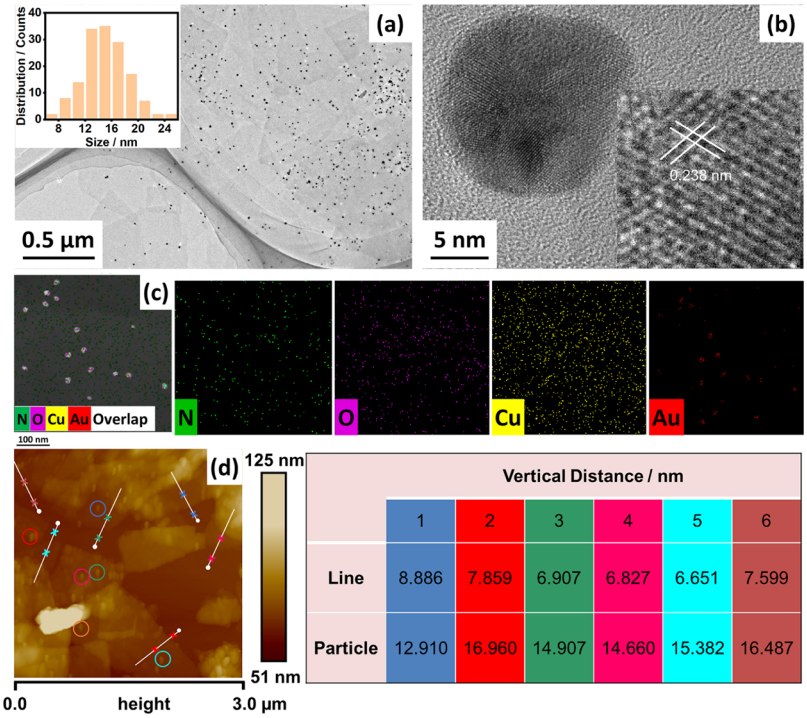

Figure 1. Morphology characterizations of ABEI/AuNPs/CuTCPP. (a) TEM image of ABEI/AuNPs/CuTCPP. Inset: histogram of size distribution of AuNPs on ABEI/AuNPs/CuTCPP. (b) TEM image of a typical AuNP on ABEI/AuNPs/CuTCPP. Inset: HRTEM of the AuNPs. (c) STEM-EDS mapping of N, O, Cu, and Au element in a selected area. (d) AFM analysis of ABEI/AuNPs/CuTCPP.

CL Measurements. The CL properties of ABEI/AuNPs/CuTCPP nanocomposites and related control solutions and nanocomposites were studied on a Centro LB 960 microplate luminometer (Berthold, Germany). Specifically, 50 μL of ABEI/AuNPs/CuTCPP or control solutions was added into a well. The CL kinetic curve was recorded when 50 μL of 1 mM H_2O_2 in 0.1 M NaOH solution was injected into the well. The measurement time was set as 30 s with a time interval of 0.1 s. The CL spectra were measured on the FL spectrometer operated with the lamp off.

Choline Determination. The determination of choline was implemented on a Centro LB 960 microplate luminometer. 50 μL of choline chloride with different concentrations was mixed well with 50 μL of 0.1 mg/mL ChO*x*. After incubation at room temperature for 6 min, the above mixtures were diluted with 3 mL of 0.1 M NaOH. Then, 50 μL of the diluent was injected into the well with 50 μL of ABEI/AuNPs/CuTCPP nanocomposites, and the CL kinetic curve was recorded in the meantime. The measurement time was set as 20 s with a time interval of 0.1 s.

RESULTS AND DISCUSSION

Synthesis and Characterizations. Synthetic routes to fabricate ABEI/AuNPs/CuTCPP nanocomposites are illustrated in Scheme 1. CuTCPP nanosheets were synthesized through the surfactant-assisted bottom-up synthetic method, followed by mixing with $HAuCl_4$ for 2 h. Then, Au(III) species were reduced *in situ* to AuNPs using ABEI as a mild reductant in the EtOH/DMF solvent, and ABEI molecules were assembled on the surface of nanosheets to form ABEI/AuNPs/CuTCPP nanocomposites.

The morphology of ABEI/AuNPs/CuTCPP nanocomposites was observed by AFM and HRTEM. CuTCPP nanosheets were flexible with smooth surface and sub-micro diameter (Figure S1). In regard to ABEI/AuNPs/CuTCPP, a large number of AuNPs with a horizontal size of 15.1 ± 3.3 nm grew on the CuTCPP substrates, which still maintained nanosheet-like nature (Figure 1a). The HRTEM image of AuNPs (Figure 1b) showed the lattice spacing of 0.238 nm, assigned to (1 1 1) planes of the fcc Au. Scanning transmission electron microscopy (STEM)−energy-dispersive system (EDS) results (Figure 1c) showed that N, O, and Cu were densely distributed throughout the whole nanosheet, and Au was deposited on the nanosheets randomly, which was well-matched with the overlap image. ICP-AES results demonstrated that the accurate amount of Cu and Au was 93.82 and 0.58 μg/mL, respectively. Similar to the HRTEM results, AFM images showed that CuTCPP exhibited 2D layered structure with the thickness of *ca.* 6.3 nm (Figure S2), and the surface of ABEI/AuNPs/CuTCPP became rough with small dots decorated on the nanosheets (Figure 1d). The vertical size of AuNPs was measured to be *ca.* 15.2 nm, which revealed that the AuNPs were quasi-spherical together with HRTEM results. The thickness of ABEI/AuNPs/CuTCPP increased to *ca.* 7.4 nm. The 1 nm increment is probably due to the multilayer stacking of ABEI molecules on CuTCPP *via* $\pi-\pi$ interactions as the estimated height of single ABEI molecule is around 0.25 nm. The elevation of absorption at *ca.* 304 nm and above *ca.* 500 nm in UV−vis spectra (Figure S3) also provided evidence that the successful assembly of AuNPs and ABEI on CuTCPP. FTIR (Figure S4) demonstrated that plenty of functional groups containing N or O existed in ABEI/AuNPs/CuTCPP nanocomposites, which could be used as heterogeneous chelation sites for the formation of AuNPs.

XPS analysis was employed to evaluate the elemental composition and chemical state of ABEI/AuNPs/CuTCPP nanocomposites. From Figure 2a, besides the five common photoelectron peaks at ∼288 eV (C 1s), ∼399 eV (N 1s), ∼533 eV (O 1s), ∼688 eV (F 1s), and 905−965 eV (Cu LMM, Cu 2p) in both CuTCPP and ABEI/AuNPs/CuTCPP, it was easy to find a new peak at ∼85 eV in ABEI/AuNPs/CuTCPP, corresponding to the characteristic Au 4f core level

https://doi.org/10.1021/acsami.1c20092
ACS Appl. Mater. Interfaces 2022, 14, 3156−3164

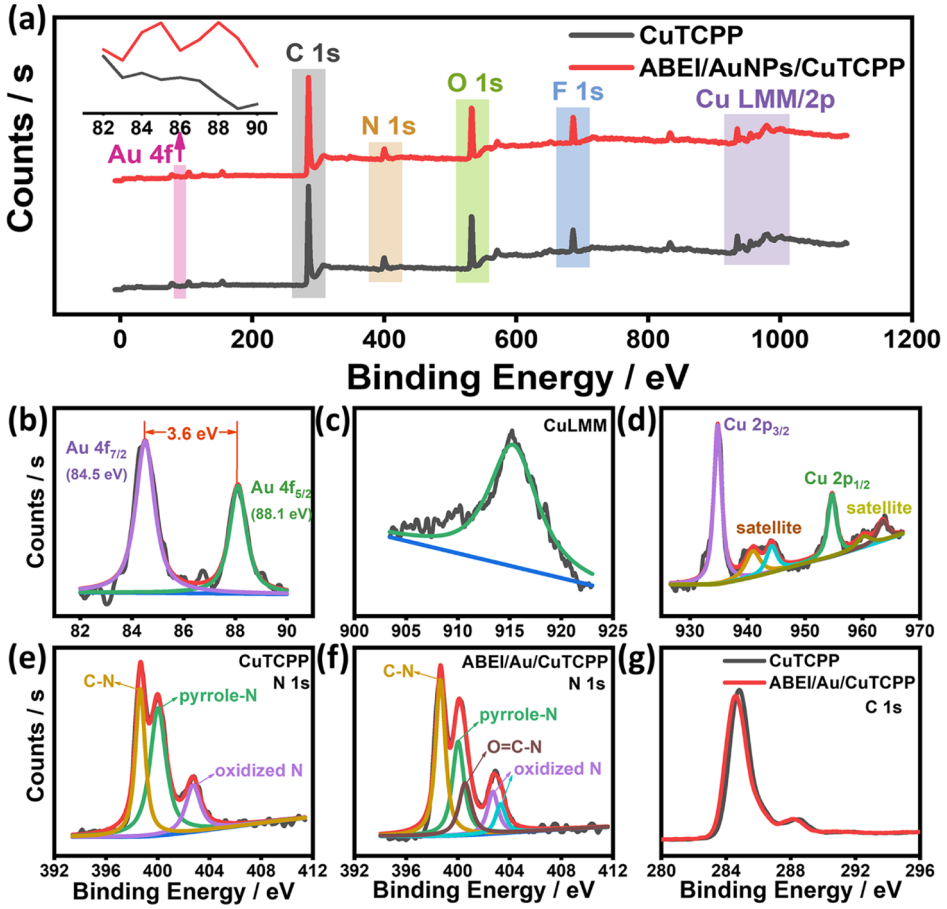

Figure 2. XPS analysis of ABEI/AuNPs/CuTCPP. (a) XPS survey spectra of CuTCPP and ABEI/AuNPs/CuTCPP. Deconvolution spectra of (b) Au 4f, (c) Cu LMM, and (d) Cu 2p of ABEI/AuNPs/CuTCPP. N 1s deconvolution spectra of (e) CuTCPP and (f) ABEI/AuNPs/CuTCPP. (g) C 1s spectra of CuTCPP and ABEI/AuNPs/CuTCPP. Inset: deconvolution of C 1s spectra of ABEI/AuNPs/CuTCPP.

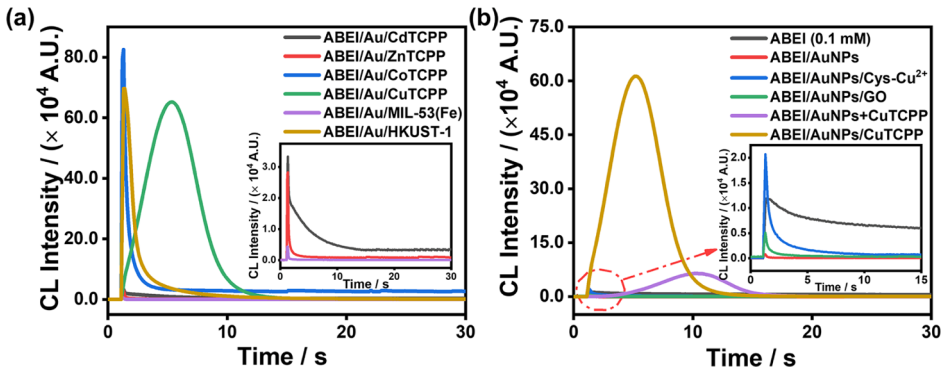

Figure 3. CL property of ABEI/Au/CuTCPP. (a) CL performance of different 2D metalloporphyrinic MOF-based nanocomposites: ABEI/AuNPs/CdTCPP, ABEI/AuNPs/ZnTCPP, ABEI/AuNPs/CoTCPP, ABEI/AuNPs/CuTCPP, ABEI/AuNPs/HKUST-1, and ABEI/AuNPs/MIL-53(Fe). Inset: magnification of CL kinetic curves of ABEI/AuNPs/CdTCPP, ABEI/AuNPs/ZnTCPP, and ABEI/AuNPs/MIL-53(Fe). (b) CL behaviors of different systems: 0.1 mM ABEI solution, ABEI/AuNPs, ABEI/AuNPs/Cys-Cu^{2+}, ABEI/AuNPs/GO, CuTCPP, and ABEI/AuNPs mixture and ABEI/AuNPs/CuTCPP. Inset: magnification of CL kinetic curves of 0.1 mM ABEI solution, ABEI/AuNPs, ABEI/AuNPs/Cys-Cu^{2+}, and ABEI/AuNPs/GO.

spectrum. Further analysis of Au 4f spectrum (Figure 2b) showed Au $4f_{7/2}$ at ~84.5 eV and Au $4f_{5/2}$ at ~88.1 eV, suggesting that Au(III) precursor was reduced to Au(0) on the nanocomposites as predicted.[24] The Cu LMM Auger spectrum (Figure 2c) at ~915.2 eV and the obvious shake-up satellites (Figure 2d) at ~940 eV in Cu $2p_{3/2}$ and ~960 eV in Cu $2p_{1/2}$ confirmed that Cu element existed in the form of Cu(II),[25] guaranteeing its high catalytic behavior on the CL reaction. Compared with the high-resolution N 1s spectrum of CuTCPP (Figure 2e,f), a new deconvolution peak at ~400.5 eV appeared in ABEI/AuNPs/CuTCPP, which was attributed to the O═C−N−N−C═O moiety of ABEI. The deconvolution C 1s spectrum (Figure 2g) showed no obvious difference between CuTCPP and ABEI/AuNPs/CuTCPP. However, the C 1s envelop of ABEI/AuNPs/CuTCPP slightly shifted toward lower binding energy by ~0.3 eV, which may be

https://doi.org/10.1021/acsami.1c20092
ACS Appl. Mater. Interfaces 2022, 14, 3156−3164

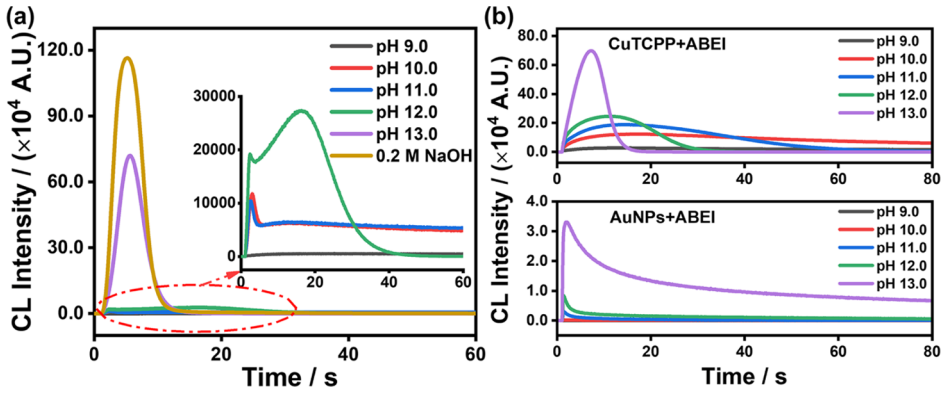

Figure 4. pH-regulated CL performance of ABEI/AuNPs/CuTCPP. (a) CL kinetic curves of ABEI/AuNPs/CuTCPP reacted with 1 mM H_2O_2 under different pH conditions. Inset: magnification of CL kinetic curves at pH 9.0−12.0. (b) CL kinetic curves of CuTCPP + ABEI (top) and AuNPs + ABEI (down) with 1 mM H_2O_2 under different pH conditions.

caused by the strong interaction between ABEI and CuTCPP plane.[26] Thus, ABEI was successfully assembled on the nanocomposites by virtue of $\pi-\pi$ interactions and weak Au−N bond.[27,28] Furthermore, XRD pattern of ABEI/AuNPs/CuTCPP (Figure S5) kept consistent with that of CuTCPP,[29,30] indicating that the structural integrity of ABEI/AuNPs/CuTCPP was well-preserved. Since CuTCPP is a porous material,[23] the surface area and porosity of ABEI/AuNPs/CuTCPP were examined by N_2 sorption experiments (Figure S6). ABEI/AuNPs/CuTCPP showed the pseudo-type-I N_2 sorption isotherms with capillary condensation at low pressures. S_{BET} was 70.2 m^2/g, which was almost 50% lower than that of CuTCPP (S_{BET} = 142.3 m^2/g), due to the effective chemisorption of ABEI on the CuTCPP nanosheets. The average pore diameter and pore volume of ABEI/AuNPs/CuTCPP was 22.8 nm and 0.354 cm^3/g, respectively.

Unique CL Property. As the dense distribution of multicatalytic sites in ABEI/AuNPs/CuTCPP, it stands to reason that ABEI/AuNPs/CuTCPP possesses excellent CL behavior. The CL curves of several functionalized 2D porphyrin-based MOFs (ABEI/AuNPs/CdTCPP, ABEI/AuNPs/ZnTCPP, ABEI/AuNPs/CoTCPP, and ABEI/AuNPs/CuTCPP) and classic 3D MOFs [HKUST-1 and MIL-53(Fe)] were plotted and are shown in Figure 3a. Under the identical measurement conditions, ABEI/AuNPs/MIL-53(Fe) ABEI/AuNPs/CdTCPP and ABEI/AuNPs/ZnTCPP showed weak CL emissions (4000−30,000 A.U.), whereas ABEI/AuNPs/HKUST-1, ABEI/AuNPs/CoTCPP, and ABEI/AuNPs/CuTCPP exhibited intense CL intensities. This is due to higher catalytic activity of Co(II) and Cu(II) centers than that of other transition-metal ions on luminol analogue reactions.[31,32] Notably, the CL kinetic curve of ABEI/AuNPs/CuTCPP presented unique and slow inverted V-shaped distribution pattern with the peak time at 5.4 s. However, the CL kinetic curve of ABEI/AuNPs/HKUST-1 and ABEI/AuNPs/CoTCPP was much rapid, which reached to the peak immediately after the injection of H_2O_2, probably owing to 3D microporous structure of HKUST-1 and much faster decomposition rate of H_2O_2 for the Co(II)-catalyzed system.[33]

The CL behaviors of different systems were studied and are shown in Figure 3b. ABEI/AuNPs/CuTCPP exhibited strongest CL emission with a peak intensity of ~650,000 A.U., nearly 60 and 10 times higher than that of ABEI at the synthetic concentration and the mixed system of CuTCPP and ABEI/AuNPs at a volume ratio of 1:1. Moreover, ABEI/AuNPs/CuTCPP possessed much greater CL activity than other CL-functionalized AuNPs or graphene-based nanomaterials like ABEI/AuNPs, ABEI/AuNPs/Cys-Cu^{2+}, and ABEI/AuNPs/GO. As displayed in Figure S7, the CL emission was reproducible with relative standard deviation (R.S.D.) of 5.5% within 10 consecutive days, demonstrating good stability of ABEI/AuNPs/CuTCPP.

During the preparation of ABEI/AuNPs/CuTCPP, PVP was utilized as the surfactant to modulate the anisotropic growth of ultrathin CuTCPP substrates, exercising profound influence on structures of ABEI/AuNPs/CuTCPP. It can be seen in Figure S8 that CL intensity of ABEI/AuNPs/CuTCPP increased appreciably with the increment of PVP and dropped slightly after $m_{PVP\text{-}K30}$ = 10 mg. Combined with TEM images (Figure S9), the morphology of CuTCPP changed from the bulky phase ($m_{PVP\text{-}K30}$ = 0 mg) to homogeneous nanosheets ($m_{PVP\text{-}K30}$ = 10 mg) and then to blurry film with wrinkles and foldings ($m_{PVP\text{-}K30}$ = 20 mg). It could be concluded that nanosheet-like CuTCPP showed higher catalytic activity. It is reported that bulky 3D MOFs would hinder mass-transfer processes and block active sites, making the reaction rate and efficiency low.[34,35] When too much PVP attached on the surface of CuTCPP, the viscosity of PVP would prevent H_2O_2 and other reactive intermediates from contacting with ABEI molecules on the CuTCPP skeleton, thus weakening the CL intensity. Likewise, the peak time variation with the amount of PVP also verified this deduction.

It is well known that the CL intensity of luminol analogue reactions is closely related to the alkalinity of H_2O_2. Interestingly, we find in this work that pH not only influences the CL intensity but also changes the kinetic curve pattern of ABEI/AuNPs/CuTCPP (Figure 4a). Weak CL phenomenon appeared at pH 9.0, and the CL intensity increased gradually with the increase in pH. Under weak alkaline medium (pH 9.0−11.0), the CL intensity of ABEI/AuNPs/CuTCPP reached its peak at 3 s and decreased quickly to a plateau. With pH 12.0, there were two segments appeared in the CL kinetic curve, where one was a spike at 3 s and another was a broad peak at 16 s. Continuing to increase the pH, the curve changed to a slow inverted V-shaped modality. We speculate that it may be related to the CL reaction rate catalyzed by different catalyst AuNPs and CuTCPP and the degradation extent of ABEI/AuNPs/CuTCPP nanocomposites in strong alkaline solutions. From Figure 4b, it can be seen that the AuNP-catalyzed ABEI-H_2O_2 system showed a faster rate with

https://doi.org/10.1021/acsami.1c20092
ACS Appl. Mater. Interfaces 2022, 14, 3156−3164

the peak time in the range of 1.4−2.1 s, whereas the CuTCPP-involved ABEI-H_2O_2 system held a delayed peak time which was concentrated in the range of 7.2−17.2 s and became earlier with increasing pH. In addition, TEM images of ABEI/AuNPs/CuTCPP after the reaction with H_2O_2 at different pH values are compared in Figure S10. The morphology of ABEI/AuNPs/CuTCPP at pH 9.0 remained unchanged, while the structure of ABEI/AuNPs/CuTCPP was broken down at pH 13.0 with blurring boundary and smaller size. Thus, the first spike can be assigned to the AuNPs-catalyzed CL emission, and the second broad peak is derived from the porous CuTCPP-contributed CL reaction. Higher pH would destroy the ABEI/AuNPs/CuTCPP structure, making the CL kinetics into an inverted V-shaped curve with only one peak.

The CL spectrum revealed that the luminophore of the ABEI/AuNPs/CuTCPP system was still ABEI molecule (Figure S11). We suggest that the uniqueness of ABEI/AuNPs/CuTCPP nanocomposites is derived from its special structural characteristics. On the one hand, AuNPs are found to facilitate the radical generation (like $OH^{\bullet}$ and $O_2^{\bullet-}$) and electron-transfer processes on the surface of AuNPs, enhancing luminol-analogue CL system,[36] and was verified to participate in the fast catalytic process in the ABEI/AuNPs/CuTCPP CL nano-system (Figure 4). On the other hand, ultrathin 2D CuTCPP nanosheets with large-surface area and numerous functional groups can function as a remarkable platform for the efficient integration of multiple molecules. The loading amount of ABEI and Cu(II) on ABEI/AuNPs/CuTCPP nanocomposites was determined to be 0.038 mM (Figure S12) and 93.82 μg/mL (ICP-AES result), respectively, which was much higher than that on most of the conventional CL-functionalized 2D nanomaterials.[37,38] What is more, the Lewis acidic nature of unsaturated Cu(II) centers on CuTCPP with high-density exposure can activate the decomposition of H_2O_2 into reactive oxygen species.[39,40] Corresponding scavengers, thiourea ($OH^{\bullet}$ inhibitor), superoxide dismutase (SOD, $O_2^{\bullet-}$ scavenger), and NaN_3 ($^1O_2$ quencher) were used to shed light on the role of these reactive oxygen species. The results, as shown in Figure S13, revealed that it was $O_2^{\bullet-}$ and $OH^{\bullet}$ rather than $^1O_2$ that contributed significantly to the ABEI/AuNPs/CuTCPP CL reaction. Furthermore, XPS analysis of Cu 2p spectra after treatment with H_2O_2 showed the existence of Cu(I) and the transformation of Cu(II) to Cu(I) during the CL reaction, as indicated by the two new peaks appeared at 932.8 and 952.8 eV (Figure S14) together with the obvious decrement in the intensity ratio of the shake-up satellite and the Cu 2p peak (Table S1),[41,42] confirming the involvement of unsaturated Cu(II) catalytic centers in ABEI/AuNPs/CuTCPP. To elaborate on the importance of CuTCPP, the CL property of the mixed system of CuTCPP and ABEI/AuNPs with different volume ratios was measured. As depicted in Figure S15, the CL intensity of the mixed system boosted dramatically with the increase in CuTCPP amount and reached the maximum at the volume ratio of 1:1, implying that CuTCPP played a distinguished role in catalysis on the ABEI CL reaction. In a word, numerous reactive oxygen species are generated with different reaction rate catalysis by the dual active centers, AuNPs and CuTCPP, of ABEI/AuNPs/CuTCPP nanocomposites, leading to the strong CL emission. Keeping the above facts in mind, the possible mechanism of the ABEI/AuNPs/CuTCPP CL reaction in alkaline solution is summarized as follows

$$\text{fast rate: } H_2O_2 \xrightarrow{\text{AuNPs}} 2HO^{\bullet}$$

$$\text{slow rate: } Cu^{II}TCPP + HO_2^- + OH^- \leftrightarrow Cu^{I}TCPP + O_2^{\bullet-} + H_2O$$

$$Cu^{I}TCPP + H_2O_2 \rightarrow Cu^{II}TCPP + HO^{\bullet} + OH^-$$

$$HO^{\bullet} + O_2 + OH^- \rightarrow H_2O_2 + O_2^{\bullet-}$$

$$ABEI^- \xrightarrow{O_2^{\bullet-},\ HO^{\bullet}} ABEI^{\bullet-}$$

$$ABEI^{\bullet-} + O_2^{\bullet-} \rightarrow ABEI_{ox}^{*}$$

$$ABEI_{ox}^{*} \rightarrow ABEI_{ox} + h\nu$$

Detection of Choline. We have found that ABEI/AuNPs/CuTCPP owns great sensitivity on H_2O_2 and possesses intrinsic peroxidase-like activity (Figure S16). Utilizing its peroxidase-mimicking activity, it is promising to achieve the effective detection of these small targets. Herein, employing choline as a model target, a CL biosensor is designed for the determination of small biomolecules (Scheme 2).

Scheme 2. Schematic Illustration of the Proposed CL Biosensor for Small Biomolecule Detection Based on ABEI/Au/CuTCPP

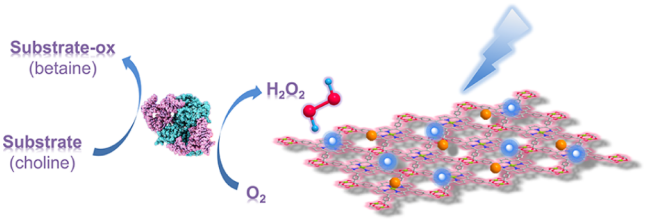

To obtain the optimum analytical performance, the key parameters, ChO*x* concentration and enzymatic reaction time, were assessed (Figure S17). Under the optimized conditions (0.1 mg/mL ChO*x*, 6 min of enzymatic reaction time), the integrated CL intensity was proportional to choline concentrations in the range of 0.3−300 μM with the regression equation of log (integrated intensity/A.U.) = 0.52 × log *C*(choline/M) + 8.14 (R^2 = 0.993), and limit of detection (LOD) was 82.6 nM (S/N = 3 and *n* = 7). R.S.D. of inter-assay and intra-assay was 3.1 and 7.6%, respectively, indicating favorable reproducibility of the proposed biosensor.

The selectivity of the proposed biosensor was evaluated using several common small molecules including acetylcholine, $NH_2OH{\cdot}HCl$, caffeine, L-cysteine, glucose, and lactic acid as interferents at a 10-fold concentration. As shown in Figure 5b, no significant CL signals are observed in the interference group compared with the blank control, except that of the target and mixture groups, indicating a high degree of anti-interference of our detection system. The proposed biosensor exhibits a lower LOD and wider liner range than most of the reported method (Table S2), mainly benefiting from the impressive nanostructures of ABEI/AuNPs/CuTCPP and the enzymatic tandem reaction from ChO*x* to peroxidase-mimetic ABEI/AuNPs/CuTCPP. Moreover, our biosensor is also simple and fast. The whole fabrication and detection procedures can be finished within 10 min.

https://doi.org/10.1021/acsami.1c20092
ACS Appl. Mater. Interfaces 2022, 14, 3156−3164

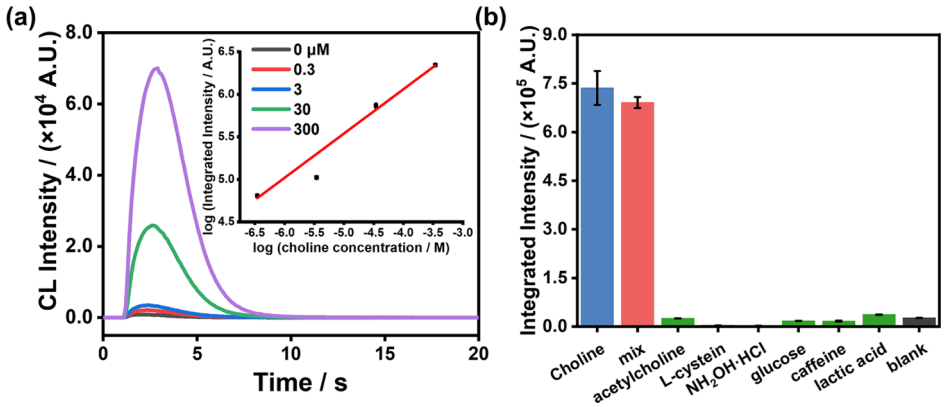

Figure 5. Analytical performance of the proposed biosensor based on ABEI/Au/CuTCPP. (a) CL responses of the proposed biosensor with different concentrations of choline. Inset: calibration curve of log (integrated intensity/A.U.) ~ log C(choline/M). (b) Selectivity of the proposed biosensor toward choline (3 μM), different interferents (0.3 μM), their mixture, and blank control.

The applicability of the proposed biosensor in real samples was investigated by recovery experiments in three healthy volunteer plasma samples. Before measuring, the samples were deproteinized by ultrafiltration (MWCO = 3 kDa) to eliminate the interference from proteins. As listed in Table 1, the original choline concentration ranged from 10.0 to 15.7 μM, which was in accordance with the literature reports.[43,44] The recoveries were in the range of 91−103% with R.S.D. of less than 5%, suggesting the promising applicability for the detection of choline in clinical samples.

Table 1. Determination of Choline in Human Serum Samples Using the Proposed Biosensor

sample no.	initially found (μM)	added[a] (μM)	totally found (μM)	recovery (%)
1	12.3 ± 0.5	10.0	22.6 ± 0.1	103
2	15.7 ± 0.2	10.0	25.3 ± 0.9	96
3	10.5 ± 0.1	10.0	19.6 ± 0.3	91

[a]The added concentration is 1−10 times the initially found concentration.

CONCLUSIONS

A CL reagent and noble metal nanoparticle dual-functionalized 2D metalloporphyrinic MOFABEI/AuNPs/CuTCPP was developed through the surfactant-assisted and *in situ* growth synthetic method. During the synthesis process, CuTCPP nanosheets served as a nanoplatform with plenty of functional groups and large specific areas, ABEI functioned as reductive reagents and CL species, Au(III) was *in situ* reduced to AuNPs, and ABEI was assembled on the surfaces of AuNPs and CuTCPP. ABEI/AuNPs/CuTCPP showed a 2D layered structure with the thickness of *ca.* 7.3 nm, and AuNPs were quasi-spherical on the nanosheets with the diameter of *ca.* 15.2 nm. ABEI/AuNPs/CuTCPP nanocomposites exhibited strong and stable CL property with the pH-regulated CL kinetic curve when reacted with H_2O_2. Under the identical measurement conditions, the CL intensity of ABEI/AuNPs/CuTCPP was 60 times higher than that of the ABEI system at synthetic concentrations and was much superior to CL-functionalized AuNPs or graphene-based nanomaterials. This excellent CL performance was mainly due to the abundant metal catalytic centers with atomic distribution of ABEI/AuNPs/CuTCPP, where AuNPs participated in the fast catalytic process and CuTCPP in the slow and strong catalytic reaction. Furthermore, ABEI/AuNPs/CuTCPP possesses intrinsic peroxidase-mimicking activity. Accordingly, ABEI/AuNPs/CuTCPP nanocomposites were employed as nanointerfaces to construct a biosensor for the detection of small molecules. The proposed biosensor showed sensitive response to choline in the linear range from 0.3 to 300 μM with a detection limit of 82.6 nM. Significantly, the strategy could be generalized to the monitoring of other metabolic processes involved in the production of H_2O_2. The strong and slow CL property may also provide interesting inspiration for the development of bioimaging.

ASSOCIATED CONTENT

Supporting Information

The Supporting Information is available free of charge at https://pubs.acs.org/doi/10.1021/acsami.1c20092.

Synthesis of 2D porphyrin-based MOFs, characterizations and CL studies of ABEI/AuNPs/CuTCPP, and detection of choline (PDF)

AUTHOR INFORMATION

Corresponding Author

Hua Cui − *CAS Key Laboratory of Soft Matter Chemistry, iChEM (Collaborative Innovation Center of Chemistry for Energy Materials), Department of Chemistry, University of Science and Technology of China, Hefei, Anhui 230026, P. R. China*; orcid.org/0000-0003-4769-9464; Phone: +86-551-63600730; Email: hcui@ustc.edu.cn; Fax: +86-551-63600730

Authors

Jue Wang − *CAS Key Laboratory of Soft Matter Chemistry, iChEM (Collaborative Innovation Center of Chemistry for Energy Materials), Department of Chemistry, University of Science and Technology of China, Hefei, Anhui 230026, P. R. China*

Chao Hu − *CAS Key Laboratory of Soft Matter Chemistry, iChEM (Collaborative Innovation Center of Chemistry for Energy Materials), Department of Chemistry, University of Science and Technology of China, Hefei, Anhui 230026, P. R. China*

Yi-sha Wang − *CAS Key Laboratory of Soft Matter Chemistry, iChEM (Collaborative Innovation Center of Chemistry for*

https://doi.org/10.1021/acsami.1c20092
ACS Appl. Mater. Interfaces 2022, 14, 3156−3164

Energy Materials), Department of Chemistry, University of Science and Technology of China, Hefei, Anhui 230026, P. R. China

Complete contact information is available at: https://pubs.acs.org/10.1021/acsami.1c20092

Author Contributions

The manuscript was written through contributions of all authors. All authors have given approval to the final version of the manuscript.

Notes

The authors declare no competing financial interest.

■ ACKNOWLEDGMENTS

The support of this research by the National Natural Science Foundation of China (grant nos. 21874122 and 21804124) and the National Key Research and Development Program of China (grant no. 2016YFA0201300) is gratefully acknowledged.

■ REFERENCES

(1) Bi, S.; Zhou, H.; Zhang, S. A Novel Synergistic Enhanced Chemiluminescence Achieved by a Multiplex Nanoprobe for Biological Applications Combined with Dual-amplification of Magnetic Nanoparticles. *Chem. Sci.* **2010**, *1*, 681−687.

(2) Chen, H.; Lin, L.; Li, H.; Li, J.; Lin, J.-M. Aggregation-Induced Structure Transition of Protein-Stabilized Zinc/Copper Nanoclusters for Amplified Chemiluminescence. *ACS Nano* **2015**, *9*, 2173−2183.

(3) Ouyang, H.; Zhang, L.; Jiang, S.; Wang, W.; Zhu, C.; Fu, Z. Co Single-Atom Catalysts Boost Chemiluminescence. *Chem.—Eur. J.* **2020**, *26*, 7583−7588.

(4) Wang, C.; Kim, J.; Tang, J.; Kim, M.; Lim, H.; Malgras, V.; You, J.; Xu, Q.; Li, J.; Yamauchi, Y. New Strategies for Novel MOF-Derived Carbon Materials Based on Nanoarchitectures. *Chem* **2020**, *6*, 19−40.

(5) Wang, S.; Wang, Q.; Feng, X.; Wang, B.; Yang, L. Explosives in the Cage: Metal-Organic Frameworks for High-Energy Materials Sensing and Desensitization. *Adv. Mater.* **2017**, *29*, 1701898.

(6) Wang, C.; Kim, J.; Tang, J.; Na, J.; Kang, Y. M.; Kim, M.; Lim, H.; Bando, Y.; Li, J.; Yamauchi, Y. Large-Scale Synthesis of MOF-Derived Superporous Carbon Aerogels with Extraordinary Adsorption Capacity for Organic Solvents. *Angew. Chem., Int. Ed.* **2020**, *59*, 2066−2070.

(7) Luo, F.; Lin, Y.; Zheng, L.; Lin, X.; Chi, Y. Encapsulation of Hemin in Metal Organic Frameworks for Catalyzing the Chemiluminescence Reaction of the H_2O_2-Luminol System and Detecting Glucose in the Neutral Condition. *ACS Appl. Mater. Interfaces* **2015**, *7*, 11322−11329.

(8) Zhu, Q.; Chen, Y.; Wang, W.; Zhang, H.; Ren, C.; Chen, H.; Chen, X. A Sensitive Biosensor for Dopamine Determination Based on the Unique Catalytic Chemiluminescence of Metal-Organic Framework HKUST-1. *Sens. Actuators, B* **2015**, *210*, 500−507.

(9) Yang, X.-L.; Chen, X.; Hou, G.-H.; Guan, R.-F.; Shao, R.; Xie, M.-H. A Multiresponsive Metal-Organic Framework: Direct Chemiluminescence, Photoluminescence, and Dual Tunable Sensing Applications. *Adv. Funct. Mater.* **2016**, *26*, 393−398.

(10) Rühle, B.; Virmani, E.; Engelke, H.; Hinterholzinger, F. M.; von Zons, T.; Brosent, B.; Bein, T.; Godt, A.; Wuttke, S. A Chemiluminescent Metal-Organic Framework. *Chem.—Eur. J.* **2019**, *25*, 6349−6354.

(11) Jiang, X.; Wang, Z.; Wang, H.; Zhuo, Y.; Yuan, R.; Chai, Y. A Novel Metal-Organic Framework Loaded with Abundant N-(aminobutyl)-N-(ethylisoluminol) as a High-Efficiency Electrochemiluminescence Indicator for Sensitive Detection of Mucin1 on Cancer Cells. *Chem. Commun.* **2017**, *53*, 9705−9708.

(12) Qin, X.; Zhang, X.; Wang, M.; Dong, Y.; Liu, J.; Zhu, Z.; Li, M.; Yang, D.; Shao, Y. Fabrication of Tris(bipyridine)ruthenium(II)-Functionalized Metal-Organic Framework Thin Films by Electrochemically Assisted Self-Assembly Technique for Electrochemiluminescent Immunoassay. *Anal. Chem.* **2018**, *90*, 11622−11628.

(13) *The Porphyrin Handbook*; Kadish, K. M., Smith, K. M., Guilard, R., Eds.; Academic Press: San Diego, 2000−2003.

(14) Zhao, M.; Huang, Y.; Peng, Y.; Huang, Z.; Ma, Q.; Zhang, H. Two-Dimensional Metal-Organic Framework Nanosheets: Synthesis and Applications. *Chem. Soc. Rev.* **2018**, *47*, 6267−6295.

(15) Zhang, F.; Zhang, J.; Zhang, B.; Zheng, L.; Cheng, X.; Wan, Q.; Han, B.; Zhang, J. CO_2 Controls the Oriented Growth of Metal-Organic Framework with Highly Accessible Active Sites. *Nat. Commun.* **2020**, *11*, 1431.

(16) Liu, X.; Yan, Z.; Zhang, Y.; Liu, Z.; Sun, Y.; Ren, J.; Qu, X. Two-Dimensional Metal-Organic Framework/Enzyme Hybrid Nanocatalyst as a Benign and m Self-Activated Cascade Reagent for in Vivo Wound Healing. *ACS Nano* **2019**, *13*, 5222−5230.

(17) Qiu, Q.; Chen, H.; Sharif, S.; You, Z.; Ying, S.; Wang, Y.; Ying, Y. Ultrathin Noble Metal Nanoplates Decorated Metal-Organic Framework Nanosheets as 2D/2D Heterojunction Nanobionic Catalysts for Explosive Residues Monitoring. *2D Mater.* **2019**, *6*, 035008.

(18) Zuo, Q.; Liu, T.; Chen, C.; Ji, Y.; Gong, X.; Mai, Y.; Zhou, Y. Ultrathin Metal-Organic Framework Nanosheets with Ultrahigh Loading of Single Pt Atoms for Efficient Visible-Light-Driven Photocatalytic H_2 Evolution. *Angew. Chem., Int. Ed.* **2019**, *58*, 10198−10203.

(19) Pfefferbaum, A.; Adalsteinsson, E.; Spielman, D.; Sullivan, E. V.; Lim, K. O. In vivo Brain Concentrations of N-acetyl Compounds, Creatine, and Choline in Alzheimer Disease. *Arch. Gen. Psychiatr.* **1999**, *56*, 185−192.

(20) Kori, M.; Aydın, B.; Unal, S.; Arga, K. Y.; Kazan, D. Metabolic Biomarkers and Neurodegeneration: A Pathway Enrichment Analysis of Alzheimer's Disease, Parkinson's Disease, and Amyotrophic Lateral Sclerosis. *OMICS A J. Integr. Biol.* **2016**, *20*, 645−661.

(21) Du, J.-J.; Yuan, Y.-P.; Sun, J.-X.; Peng, F.-M.; Jiang, X.; Qiu, L.-G.; Xie, A.-J.; Shen, Y.-H.; Zhu, J.-F. New Photocatalysts Based on MIL-53 Metal-Organic Frameworks for the Decolorization of Methylene Blue Dye. *J. Hazard. Mater.* **2011**, *190*, 945−951.

(22) Al-Janabi, N.; Hill, P.; Torrente-Murciano, L.; Garforth, A.; Gorgojo, P.; Siperstein, F.; Fan, X. Mapping the Cu-BTC Metal-Organic Framework (HKUST-1) Stability Envelope in the Presence of Water Vapour for CO_2 Adsorption from Flue Gases. *Chem. Eng. J.* **2015**, *281*, 669−677.

(23) Zhao, M.; Wang, Y.; Ma, Q.; Huang, Y.; Zhang, X.; Ping, J.; Zhang, Z.; Lu, Q.; Yu, Y.; Xu, H. J. A. M. Ultrathin 2D Metal-Organic Framework Nanosheets. *Adv. Mater.* **2015**, *27*, 7372−7378.

(24) Jaramillo, T. F.; Baeck, S. H.; Roldan Cuenya, B.; McFarland, E. W. Catalytic Activity of Supported Au Nanoparticles Deposited from Block Copolymer Micelles. *J. Am. Chem. Soc.* **2003**, *125*, 7148−7149.

(25) McIntyre, N. S.; Cook, M. G. X-Ray Photoelectron Studies on Some Oxides and Hydroxides of Cobalt, Nickel, and Copper. *Anal. Chem.* **1975**, *47*, 2208−2213.

(26) Zhang, L.; Peisert, H.; Biswas, I.; Knupfer, M.; Batchelor, D.; Chassé, T. Growth of Zinc Phthalocyanine onto ZnS Film Investigated by Synchrotron Radiation-Excited X-ray Photoelectron and Near-Edge Absorption Spectroscopy. *Surf. Sci.* **2005**, *596*, 98−107.

(27) Cui, H.; Wang, W.; Duan, C.-F.; Dong, Y.-P.; Guo, J.-Z. Synthesis, Characterization, and Electrochemiluminescence of Luminol-reduced Gold Nanoparticles and Their Application in a Hydrogen Peroxide Sensor. *Chem.—Eur. J.* **2007**, *13*, 6975−6984.

(28) Tian, D.; Zhang, H.; Chai, Y.; Cui, H. Synthesis of N-(aminobutyl)-N-(ethylisoluminol) Functionalized Gold Nanomaterials for Chemiluminescent Bioprobe. *Chem. Commun.* **2011**, *47*, 4959−4961.

(29) Makiura, R.; Motoyama, S.; Umemura, Y.; Yamanaka, H.; Sakata, O.; Kitagawa, H. Surface Nano-Architecture of a Metal-Organic Framework. *Nat. Mater.* **2010**, *9*, 565−571.
(30) Xu, G.; Yamada, T.; Otsubo, K.; Sakaida, S.; Kitagawa, H. Facile "Modular Assembly" for Fast Construction of a Highly Oriented Crystalline MOF Nanofilm. *J. Am. Chem. Soc.* **2012**, *134*, 16524−16527.
(31) Klopf, L. L.; Nieman, T. A. Effect of Iron(II), Cobalt(II), Copper(II), and Manganese(II) on the Chemiluminescence of Luminol in the Absence of Hydrogen Peroxide. *Anal. Chem.* **1983**, *55*, 1080−1083.
(32) Wang, J.; Zhong, W.; Liu, X.; Yang, T.; Li, F.; Li, Q.; Cheng, W.; Gao, C.; Jiang, Z.; Jiang, J. Highly Active Graphene Oxide-Supported Cobalt Single-Ion Catalyst for Chemiluminescence Reaction. *Anal. Chem.* **2017**, *89*, 13518−13523.
(33) Hanaoka, S.; Lin, J.-M.; Yamada, M. Chemiluminescent Flow Sensor for H_2O_2 Based on the Decomposition of H_2O_2 Catalyzed by Cobalt(II)-Ethanolamine Complex Immobilized on Resin. *Anal. Chim. Acta* **2001**, *426*, 57−64.
(34) Ghalei, B.; Sakurai, K.; Kinoshita, Y.; Wakimoto, K.; Isfahani, A. P.; Song, Q.; Doitomi, K.; Furukawa, S.; Hirao, H.; Kusuda, H.; Kitagawa, S.; Sivaniah, E. Enhanced Selectivity in Mixed Matrix Membranes for CO_2 Capture through Efficient Dispersion of Amine-Functionalized MOF Nanoparticles. *Nat. Energy* **2017**, *2*, 17086.
(35) Hu, W. C.; Younis, M. R.; Zhou, Y.; Wang, C.; Xia, X. H. In Situ Fabrication of Ultrasmall Gold Nanoparticles/2D MOFs Hybrid as Nanozyme for Antibacterial Therapy. *Small* **2020**, *16*, 2000553.
(36) Zhang, Z.-F.; Cui, H.; Lai, C.-Z.; Liu, L.-J. Gold Nanoparticle-Catalyzed Luminol Chemiluminescence and Its Analytical Applications. *Anal. Chem.* **2005**, *77*, 3324−3329.
(37) Li, Q.; Li, F.; Shen, W.; Liu, X.; Cui, H. Lucigenin/Co(tryptophan)$_2$ Complex Bifunctionalized Graphene Oxide: Facile Synthesis and Unique Chemiluminescence. *J. Mater. Chem. C* **2016**, *4*, 3477−3484.
(38) Han, Z.; Li, F.; Shu, J.; Gao, L.; Liu, X.; Cui, H. Acridinium Ester-Functionalized Carbon Nanomaterials: General Synthesis Strategy and Outstanding Chemiluminescence. *ACS Appl. Mater. Interfaces* **2016**, *8*, 17454−17460.
(39) Sigel, H.; Fliere, C.; Grisser, R. On the Kinetics and Mechanism of the Decomposition of Hydrogen Peroxide Catalyzed by the Cu^{2+}–2, 2'-Bipyridyl Complex. *J. Am. Chem. Soc.* **1969**, *91*, 1061−1064.
(40) Hureau, C.; Faller, P. Aβ-mediated ROS Production by Cu Ions: Structural Insights, Mechanisms and Relevance to Alzheimer's Disease. *Biochimie* **2009**, *91*, 1212−1217.
(41) Martínez, J. M. L.; Rodriguez-Castellon, E.; Sanchez, R. M. T.; Denaday, L. R.; Buldain, G. Y.; Orto, V. C. D. XPS Studies on the Cu(I,II)-Polyampholyte Heterogeneous Catalyst: An Insight into Its Structure and Mechanism. *J. Mol. Catal. A: Chem.* **2011**, *339*, 43−51.
(42) Li, X.; Liu, S.; Cao, D.; Mao, R.; Zhao, X. Synergetic Activation of H_2O_2 by Photo-Generated Electrons and Cathodic Fenton Reaction for Enhanced Self-Driven Photoelectrocatalytic Degradation of Organic Pollutants. *Appl. Catal., B* **2018**, *235*, 1−8.
(43) Hirsch, M. J.; Growdon, J. H.; Wurtman, R. J. Relations between dietary choline or lecithin intake, serum choline levels, and various metabolic indices. *Metabolism* **1978**, *27*, 953−960.
(44) Ulus, I. H.; Özyurt, G.; Korfali, E. Decreased Serum Choline Concentrations in Humans after Surgery, Childbirth, and Traumatic Head Injury. *Neurochem. Res.* **1998**, *23*, 727−732.

https://doi.org/10.1021/acsami.1c20092
ACS Appl. Mater. Interfaces 2022, 14, 3156−3164